Miniaturized 24GHz FMCW Radar Leakage Mitigation with Synchronized Subtraction

Han-Sol Kim, Jiyeol Meang, Ju-Hye Kim, Dong-Sik Ko, Seong-Ho Seo, Muhammad Tayyab Azim and Seong-Ook Park, *Senior Member*

***Abstract*—Frequency-modulated continuous wave (FMCW) radar sensors are widely used to measure range, velocity, and target status. As the range of applications for FMCW radar sensors expands, there is an increasing demand for smaller FMCW radar sensors suitable for use in confined spaces. To reduce the form factor of the FMCW radar sensor, the distance between the transmit (Tx) and receive (Rx) antennas is also reduced. This decrease in antenna separation increases the magnitude of the leakage signal transmitted from the Tx to the Rx antenna. However, the leakage signal makes it difficult for the FMCW radar sensor to detect the target by increasing the noise floor. In this article, we present an advanced method to mitigate the increased leakage signal power in the miniaturized FMCW radar sensor. We have fabricated a miniaturized homodyne FMCW radar with consistent leakage signal characteristics. We also propose a method to minimize the influence of the leakage signal by storing the leakage signal characteristics and using the stored data when operating the radar. Experimental results show significant leakage signal power reduction. This technique not only preserves the power of the received target signals but also improves the overall performance of compact FMCW radar sensors. The proposed method provides a basis for miniaturized radar sensors to contribute to various industries by providing an effective solution to the leakage signal problem of small radar technology.**

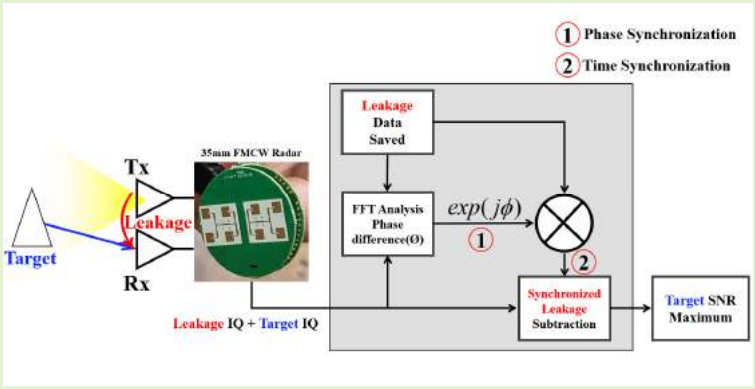

***Index Terms*—Leakage signal, frequency-modulated continuous wave (FMCW) radar sensor, miniaturization, time-synchronized, phase-synchronized, signal to noise ratio (SNR), homodyne, noise floor, subtraction, digital signal processing, phase noise.**

I. Introduction

RADAR, known for its ability to operate in adverse weather conditions and at night, is widely used for target detection [1]. Its reliability makes it an indispensable sensor in situations where consistent performance is essential. Two types of radar are commonly used. Depending on how they transmit and receive radio waves, there are pulse radar and frequency-modulated continuous wave (FMCW) radar. Pulse radar transmits for short periods of time, but is not suitable for short-range detection because it cannot receive signals while transmitting. It means that the deactivation of the receiver during pulse transmission limits the minimum measurable range, making it blind at short ranges. In contrast, FMCW radar transmits and receives signals continuously, which is ideal for short-range target detection [2]. There are two architectures of FMCW radar systems: Heterodyne and Homodyne. Heterodyne radar forms the beat signal in the intermediate frequency (IF) stage, so it requires an additional band pass filter (BPF), local oscillator (LO) and many components for implementation, which increases power consumption and device area. On the other hand, homodyne radar directly mixes the reference signal and the received signal to generate a baseband beat signal without an IF stage. Therefore, homodyne radar has a relatively simple structure and requires fewer components than heterodyne radar [3]-[4].

In contrast to past radar systems, which were large and complex, the development of semiconductor technology, advancements in radio frequency (RF) circuit fabrication, and improvements in central processing unit (CPU) performance have facilitated the miniaturization of radar systems [5]. These technological advances have enabled the development of

Manuscript received 31 January 2024. This work was supported in part by Research and Development of an FMCW-type sensor system that minimizes the effects of surrounding clutter and noise funded by the Poongsan Defense Industry Research Institute under Grant G01230079.

Han-Sol Kim is with the School of Electrical Engineering, Korea Advanced Institute of Science and Technology, Daejeon 34141, South Korea (e-mail:gksthf30638@kaist.ac.kr).

Ji-Yeol Meang is with the smartphone R&D group, Samsung Electronics , Suwon 16677, South Korea (e-mail:meang94@gmail.com)

Ju-Hye Kim, Dong-Sik Ko, Seong-Ho Seo are with the Poongsan Defense Industry Research Institute, Daejeon 34027, South Korea (e-mail:jukim@poongsan.co.kr; abito99@poongsan.co.kr; seong-ho.seo@poongsan.co.kr;).

Muhammad Tayyab Azim, Seong-Ook Park are with the School of Electrical Engineering, Korea Advanced Institute of Science and Technology, Daejeon 34141, South Korea (e-mail:tayyabazim@kaist.ac.kr;soparky@kaist.ac.kr).

compact radar systems that consume less power and are suitable for short-range detection applications. Therefore, the FMCW type, ideal for short-range detection, has been predominantly selected for small radar systems. In addition, the homodyne architecture has been selected because of its simple structure and suitability for integration on small circuit boards. Because of its diverse advantages, the FMCW homodyne radar sensors are increasingly used in various industrial applications [6]. For instance, the FMCW radar sensors are used for surveillance [7] and serve as important tools in monitoring vehicle density on roadways [8]. While not as sophisticated as optical sensors that can detect the quality of a person's sleep [9] or measure very minute amounts of histamine [10], radars are also used as sensors for human recognition, heart rate measurement, and human health monitoring [11]-[13]. In addition, radar sensors play a pivotal role in autonomous driving applications when integrated with cameras and Light Detection and Ranging (LiDAR) systems [14].

As in the case presented above, the small size of the FMCW homodyne radar sensor makes it very versatile for many applications. However, as the size of the FMCW radar sensor is reduced, the chronic problem of leakage signals occurs [6], [15]-[17]. The reduced distance between the transmit (Tx) antenna and the receive (Rx) antenna increases the magnitude of the leakage signals. These leakage signals consist of low-frequency signals and DC components. The problem of leakage signal is that its frequency is similar to the target signals for short-range detection. Consequently, the increased power of the leakage signals can significantly impede the radar performance to identify the target frequencies, thereby complicating the target detection process [17]. In addition, compact small radar sensors typically use microcontroller units (MCU) with relatively lower performance capabilities than conventional radar systems. The use of MCUs with limited memory capacity and lower analog-to-digital converter (ADC) sampling rates poses challenges. These limitations become particularly evident when lower sampling rates reduce signal resolution. Such a reduction in resolution can complicate the distinction between target signals and background noise, thereby impacting the overall performance of the sensor in reliably detecting targets. In summary, the increased leakage signal of miniaturized FMCW radar sensors contributes to the degradation of sensor performance.

Various methods have been proposed to mitigate the leakage signals in FMCW radar. One method was to increase the distance between the Tx and Rx antennas using fiber optic cable [18] and long coaxial cables to mitigate the leakage signals [19]. In addition, the power of the leakage signals was attenuated by placing a wall between the antennas [20]. More advanced approaches involved analyzing the amplitude and phase of system-generated leakage signals over a period of time and then generating appropriate adaptive signals using hardware or digital modules [21]-[22]. Balanced topologies, applicable in radar front-ends, have been proposed to cancel the leakage signal [23]-[24]. In addition, the noise of the signal reflected from the object in front of the antenna was defined as short-range leakage, and a similar signal was generated on board artificially at the RF stage and then subtracted at the IF stage to mitigate the leakage signal [25]-[26]. Reference [27] statistically modeled noise and applied background subtraction based on this modeling to attenuate leakage signals. A technique introduced in [15]-[16] is to digitally shift the frequency of the leakage signal directly to DC to minimize the influence of the phase noise of the leakage signal from the heterodyne structure, thus improving the target signal-to-noise ratio (SNR). Recently, hybrid analog-digital compensation techniques have been proposed to mitigate leakage signals and stationary clutter in short-range FMCW radar [17].

However, approaches such as [18]-[20] become less practical as system volume increases and requires a large space for operation. Methods that involve the generation and removal of analog or digital signals similar to leakage signals also require additional hardware. Furthermore, the process of creating a target in front of the radar sensor also requires the insertion of chip-level hardware. In addition, the leakage signal modeling in [27] requires complicated computational processes that are unsuitable for small radar sensors with limited memory capacity. The technique proposed in [15]-[16] focuses on mitigating the leakage phase noise from using multiple oscillators in heterodyne FMCW radar structures. However, homodyne FMCW radar sensors that use a single oscillator exhibit fewer phase noise levels than heterodyne FMCW radar systems. While the method in [17] facilitates the subtraction of leakage signals by aligning time synchronization, we find it insufficient in miniaturized FMCW radar sensors. In addition, the method presented in [17] uses an approach that includes externally injected signals, which increases hardware complexity. Therefore, this method is not suitable for application in small radar sensors.

We proposed a novel approach to mitigate the leakage signal of miniaturized radar sensors by time- and phase-synchronized leakage subtraction. To verify the proposed method, we fabricated a miniaturized K-band FMCW radar sensor. Unlike the conventional sawtooth FMCW radar, we changed the frequency sweep pattern to minimize the noise in the baseband. We also applied a sophisticated control mechanism to make a coherent radar sensor. As a result, the radar sensor can maintain consistent coherence in the baseband signals over time. To mitigate the leakage signal in a miniaturized radar sensor, we pre-store the in-phase and quadrature (IQ) data about the leakage signal. However, there is a phase difference between the stored leakage signal data and the leakage signal data generated during operation. By eliminating the phase difference and implementing time synchronization, we can subtract the time- and phase-synchronized leakage signal data from the leakage signal data. Thus, we significantly attenuate the power of the leakage signal in a miniaturized radar sensor. We present the results of three experiments to validate the proposed leakage attenuation method in a compact FMCW radar sensor. The first experiment shows a significant reduction in leakage signal power and noise floor. The second experiment involves a drone (DJI Inspire 2) with a very low radar cross-section (RCS) $0.01m^2$ and evaluates the improvement in SNR. The third experiment is extended to targets with higher RCS $0.22m^2$. Unlike the methods in [17], [20]-[22], [25]-[26], the proposed method does not require any additional hardware. All digital signal processing (DSP) and data storage in our experiments are performed using MATLAB R2023a.

The contents of this article are as follows. Section II presents

the theories of FMCW radar and the signal model in FMCW homodyne radar. Section III presents the design of the proposed system and a detailed description of the proposed method. Section IV shows the fabricated FMCW radar sensor and outlines the experimental setup. Section V shows the results of applying the proposed algorithm through outdoor experiments and conducts a comparative analysis. Section VI compares the proposed method with a recent leakage mitigation method. Section VI deals with the conclusions.

II. THEORY

A. FMCW Radar Principle.

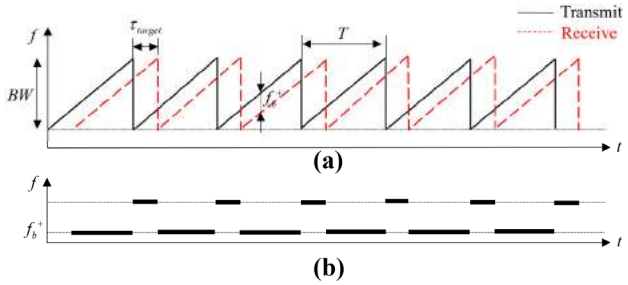

Fig. 1. Linear sawtooth FMCW waveform with stationary target. (a) Frequency of transmitted and received ramp chirps as a function of time. (b) The resulting beat frequency as a function of time.

FMCW radar continuously transmits a signal whose frequency varies linearly with duration time (T). This linear frequency modulation (LFM) signal, known as a chirp signal, is a sinusoidal wave. BW is the frequency difference between the upper frequency and the lower frequency. Because the waveforms continuously transmitted by an FMCW radar exhibit a sawtooth pattern of frequency values over time, these systems are classified as sawtooth FMCW radars. When the sawtooth FMCW radar transmits a chirp signal as illustrated in Fig. 1(a), it receives the reflected chirp signal from the target after the delay time (τ_{target}). The received signal is mixed with the reference signal, resulting in the generation of a beat frequency (f_b^+) that corresponds to the frequency difference between the transmitted and received signals, as illustrated in Fig. 1(b). This frequency difference enables the FMCW radar to measure round-trip delay to the target. Multiplying this delay time by the speed of light (c) calculates the target range. The target range (R_{target}) can be expressed as follows:

$$R_{target} = \frac{c \times \tau_{target}}{2} \tag{1}$$

B. Signal Model in FMCW Homodyne Radar Sensor

Fig. 2 shows the block diagram of a homodyne FMCW radar system. The phase-locked loop (PLL) circuit, including the oscillator, generates the chirp signal. The chirp signal passes through a divider and is split into two paths. On one path, the chirp signal passes through a power amplifier (PA) before being radiated by an antenna. On the other path, which serves as the reference signal ($S_{reference}$), the chirp signal passes through

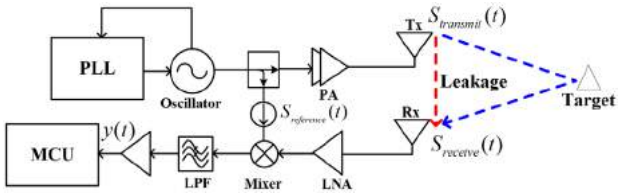

Fig. 2. Block diagram of homodyne FMCW radar.

an isolator and is sent to the mixer in the receiver for down-conversion. Patch antennas, with their small form factor, are well-suited for applications involving small radar sensors. Nonetheless, the limited bandwidth of patch antennas may result in amplitude inconsistencies during the transmission of chirp signals. Consequently, the mathematical expression for the radiated signal through the patch antenna and the chirp signal for the reference signal can be expressed as follows:

$$S_{transmit}(t) = A_{TX}(t)\cos(2\pi f_{TX} t + \pi k t^2 + \theta_1 + \varphi_1(t)) \tag{2}$$

$$S_{reference}(t) = A\cos(2\pi f_{TX} t + \pi k t^2 + \theta_1' + \varphi_1'(t)) \tag{3}$$

for $0 < t < T$, where $A_{TX}(t), A$ and f_{TX} represent the amplitude and start frequency of the chirp signal, respectively. k represents the slope of the chirp $\left(k = \frac{BW}{T}\right)$. θ_1, θ_1' and $\varphi_1(t), \varphi_1'(t)$ correspond to the fixed phase and phase noise of the radiated chirp signal and the reference signal, respectively. Most of the chirp signal radiated by the Tx antenna travels toward the target. However, a portion of the radiated signal is received directly by the Rx antenna. This signal, which is delayed by the distance between the Tx and Rx antennas, is called the leakage signal. Additionally, the Rx antenna receives the signal delayed by the distance between the target and the radar sensor. These signals pass through the low-noise amplifier (LNA) and then to the mixer for down-conversion. The received signals can be expressed as follows:

$$\begin{aligned} S_{receive}(t) = & \underbrace{A_{leakage}'(t)\cos\left(2\pi f_{RX}(t-\tau_{leakage}) + \pi k(t-\tau_{leakage})^2 + \theta_2' + \varphi_2(t)\right)}_{leakage\ signal} \\ & \underbrace{+A_{target}'(t)\cos\left(2\pi f_{RX}(t-\tau_{target}) + \pi k(t-\tau_{target})^2 + \theta_3' + \varphi_3(t)\right)}_{target\ signal} \end{aligned} \tag{4}$$

for $0 < t < T$, where $A_{leakage}'(t), A_{target}'(t)$ and $f_{RX}(= f_{TX})$ represent the amplitude and start frequency of received leakage and target signal, respectively. θ_2', θ_3' and $\varphi_2(t), \varphi_3(t)$ correspond to the fixed phase and phase noise of the received leakage and target signal, respectively. $\tau_{leakage}$ is the total internal delay between the Tx to Rx antenna path. τ_{target} signifies the round-trip delay to the target. The received signals are down-converted after mixing with the reference signal. The down-converted signal passes through a low-pass filter (LPF). These signals then pass through an amplifier before being

passed to the ADC within the MCU chip. The signals $y(t)$ before the MCU chip can be expressed as follows:

$$\begin{aligned} y(t) &= \left[S_{reference}(t) \times S_{receive}(t) \right] * h_{LPF}(t) \\ &= \underbrace{A_{leakage}(t)\cos\left(2\pi k\tau_{leakage}t + \theta_2 + \varphi_1(t) - \varphi_2(t)\right)}_{leakage\ signal} \\ &\quad + \underbrace{A_{target}(t)\cos\left(2\pi k\tau_{target}t + \theta_3 + \varphi_1(t) - \varphi_3(t)\right)}_{target\ signal} \end{aligned} \quad (5)$$

for $0 < t < T$, where $A_{leakage}(t), A_{target}(t)$ represent the amplitude of the received leakage and target baseband signal, respectively. De-ramping occurs when the received signal is mixed with the reference signal. This process results in the generation of a beat signal. The frequency of this beat signal can be characterized as a singular frequency that represents the frequency difference between the received and reference signals. Therefore, $k\tau_{leakage}$, $k\tau_{target}$ represent the beat frequency of the received leakage and target signals, respectively. θ_2, θ_3 and $\varphi_1(t) - \varphi_2(t)$, $\varphi_1(t) - \varphi_3(t)$ correspond to the fixed phase and phase noise of the received leakage beat signal and the target beat signal, respectively. In the homodyne FMCW radar, since the same oscillator generates both the transmitted and reference signals, the phase noise in these signals is correlated. Therefore, the phase noise magnitude of the leakage signal after de-ramping is significantly reduced because of the range correlation effect [15]. This reduction occurs because the leakage signal, which has a small delay, self-cancels the phase noise in the received and reference signals. As a result, the phase noise of the leakage signal in $y(t)$ shows minimal variation. In summary, the de-ramped signal $y(t)$ can be expressed as follows:

$$\varphi_1(t) - \varphi_2(t) = \underbrace{\varphi_1(t) - \varphi_1(t - \tau_{leakage})}_{Range\ correlation\ effect} \cong 0 \quad (6)$$

$$\begin{aligned} y(t) &\cong \underbrace{A_{leakage}(t)\cos\left(2\pi k\tau_{leakage}t + \theta_2\right)}_{leakage\ signal} \\ &\quad + \underbrace{A_{target}(t)\cos\left(2\pi k\tau_{target}t + \theta_3 + \varphi_1(t) - \varphi_3(t)\right)}_{target\ signal} \end{aligned} \quad (7)$$

III. Proposed and Realization Method

A. Small Radar Sensor With a Diameter of 35 mm

We designed a miniaturized homodyne FMCW radar sensor with a diameter of 35 mm. As there was limited space for components, we made two different printed circuit boards (PCB) to accommodate all components of the radar sensor. A block diagram of two PCBs is shown in Fig. 3. We divided the roles into two 35 mm diameter PCBs, which enable the operation of the radar sensor through interconnection. The first-floor PCB was designed to supply power, control the radar sensor through the MCU chip, store IQ data, and process the target range estimation algorithm. The second-floor PCB operates under the control signals of the serial peripheral

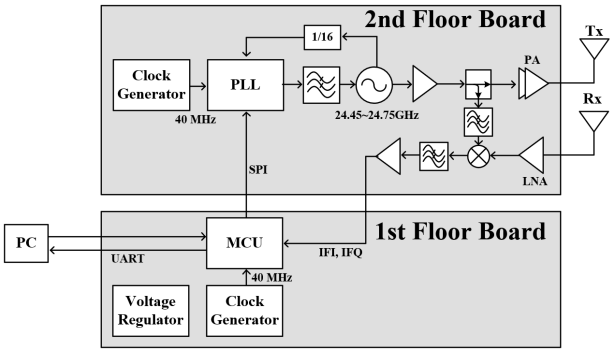

Fig. 3. Block diagram of miniaturized K-band homodyne FMCW radar sensor.

interface (SPI) communication in the MCU. Its primary function is to generate and radiate K-band signals. To generate a K-band signal, the second-floor signal generator uses a delta-sigma modulated N-PLL chip. It allows fractional-N division, which enables precise frequency tuning. This feature is ideal for applications requiring wide bandwidth and high-frequency resolution. After the PLL chip, the signal is converted to a K-band signal by a voltage-controlled oscillator (VCO) within the 24GHz transceiver. The K-band signal passes through a series of components, such as a divider and PA, before being transmitted by the Tx patch antenna. In some cases, Vivaldi antennas have been used to minimize the antenna size and maximize the gain [28]. However, we have designed and

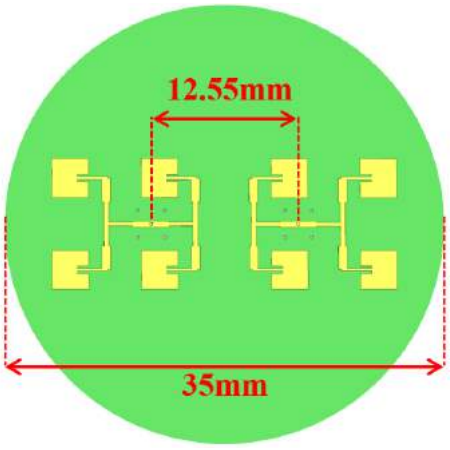

Fig. 4. Patch antenna of K-band homodyne FMCW radar sensor.

TABLE I
Parameters of Antenna Simulation Results

Parameters	Values
Operating frequency	24.45-24.75 GHz
Bandwidth	300 MHz
Radiation Efficiency	71.61 %
Isolation	-25 dB
Gain	11.56 dBi
3dB E-plane Beam width	36.4 °
3dB H-plane Beam width	40.8 °

used patch antenna to radiate in the boresight on a 35mm substrate, as depicted in Fig. 4. In the compact design of our small-sized FMCW radar sensor, the antenna configuration was oriented towards maximizing gain rather than focusing on Tx-Rx isolation. This design was driven by the limitations of the reduced PCB space, which often requires a trade-off between antenna gain and isolation. To address the issue of isolation, we implemented a system synchronization method and phase-synchronized subtraction to increase the SNR of the target. The antenna parameters are presented in Table I. The Rx antenna receives the signal reflected from the target and the leakage signal. After passing through the LNA, the received signals are mixed with reference signals and filtered to produce analog baseband signals. After de-ramping, it passes through a differential amplifier and filter. Finally, the baseband signal is converted to digital data by an ADC in the MCU and stored in memory.

B. Coherent Small Radar Sensor

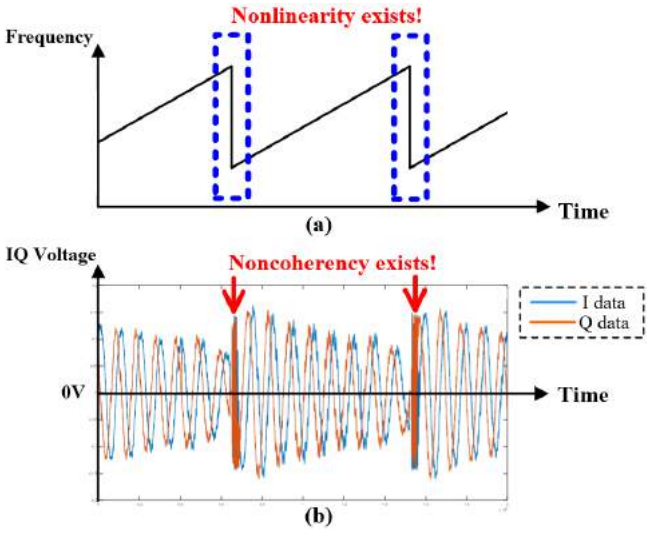

Fig. 5. Linear sawtooth conventional FMCW waveform with no target. (a) Frequency of transmitted ramp chirps as a function of time. (b) The resulting noncoherent leakage IQ data as a function of time.

In conventional sawtooth FMCW radar systems, a continuous sequence of chirp signals is generated. Following the radiation of these chirp signals, the baseband IQ signal is sequentially sampled by an ADC, as shown in Fig. 5. We experimented with a conventional sawtooth FMCW radar system to obtain the baseband leakage IQ signal. We set the Tx and Rx antennas to point toward the sky to receive only leakage signals. Fig. 5(a) illustrates the linear frequency increase of the chirp signal in the time domain. Fig. 5(b) shows the resulting baseband leakage IQ signal in the time domain. As demonstrated in Fig. 5(b), the coherence of the leakage IQ signal is inconsistent for each chirp. This is because of the nonlinear characteristics of the PLL as it moves from upper to lower frequency bands in signal generation. The nonlinearity in the PLL causes randomness at the beginning of each chirp due to the difference in phase lock time chirp to chirp. Consequently, when the PLL generates a chirp signal, as illustrated in Fig. 5(a), a noisy signal is generated at the end of the chirp and the beginning of the next chirp. In addition, the non-coherence results in different phases of the leakage IQ signal over different chirps in conventional sawtooth FMCW radar.

To create a compact and coherent FMCW radar sensor, we synchronize the generation and radiation of chirp signals with the sampling of ADC at the baseband stage. Initially, the MCU, PLL, and transceiver chip are configured to the desired specifications via SPI communication. After the initial configuration, MCU sends a short trigger1 signal to the PLL chip to operate the radar. In response to trigger1, the PLL generates a trigger2 signal, which is separated into two paths, as depicted in Fig. 6. Trigger2 makes the transceiver radiate a K-band signal, and at the same time, MCU performs the sampling via ADC. This timing synchronization works to

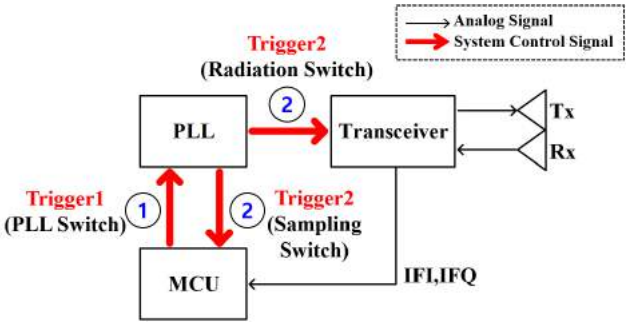

Fig. 6. System control mechanism for coherent FMCW radar sensor.

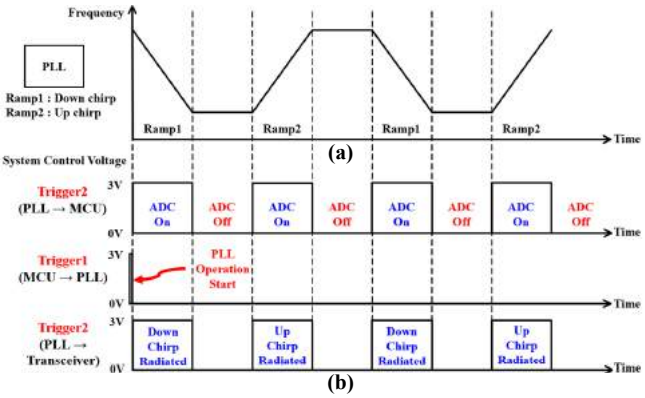

Fig. 7. FMCW radar sensor operation for coherent FMCW radar sensor as a function of time. (a) The frequency of transmitted ramp chirps as a function of time. (b) The system control signal for coherency as a function of time.

maintain coherent radar sensor operation between chirps.

To minimize the PLL nonlinearity during signal generation, the frequency sweep plan differs from conventional FMCW sawtooth radar, as illustrated in Fig. 7(a). After each chirp signal is generated, the system includes a rest period. This reduces sudden frequency transitions, a major cause of nonlinearity in the PLL. When the PLL receives the short trigger1 signal from the MCU for radar operation, the PLL immediately begins to generate a down chirp signal by interacting with the VCO in the transceiver. The bandwidth or duration of the chirp is based on the value previously written

via SPI communication. When the PLL and VCO start generating the chirp signal, the PLL generates a system control DC signal (trigger2) of the same length as the chirp duration as illustrated in Fig. 7(b). Simultaneously, PLL sends the control signal to the transceiver and MCU. This trigger2 signal acts as a switch and controls the start and end of K-band signal generation in the transceiver. Also, the trigger2 signal governs the start and end of ADC sampling in the MCU. Therefore, the efficiency in power and memory is high because the transceiver radiates and MCU samples only when the chirp is generated. In addition, the noise caused by the difference in PLL lock time is reduced by the frequency sweep illustrated in Fig. 7(a).

C. Leakage Subtraction Scheme

By implementing the consistency of system operation and changing the frequency sweep, the FMCW radar sensor can produce every chirp signal with consistent characteristics. This ensures that the FMCW radar sensor can maintain coherency in its baseband signal for each chirp. Then, the baseband leakage signal of the miniaturized radar sensor is also coherent. Therefore, the leakage IQ data of the miniaturized radar sensor can be stored in advance and used to subtract and mitigate the leakage signal. When the radar sensor operates, leakage mitigation can be effectively obtained by subtracting the pre-stored leakage IQ data from the received IQ data in the sampled time domain. To store the radar leakage IQ data, it is necessary to create an environment where only the leakage signal is present. This is typically not feasible in the operating environment where radar sensors are commonly used. Therefore, pointing the radar to the sky is used to ensure a pure leakage signal environment.

In addition, there is one more thing to consider before subtracting the pre-stored leakage IQ data from the received IQ data in the sampled time domain. The operating environments for radar sensors differ from those in which the leakage IQ data are saved. The radar sensor needs to operate after collecting the leakage signal data in advance. This discrepancy requires a system restart (power off and on cycles) during which subtle variations in the constant phase of the leakage signal may occur. This can be due to several factors, including thermal changes [29], electronic component settling times, and minor instabilities in the oscillator or other electronic components during power-up. Therefore, considering the phase difference between the leakages before subtraction is essential to minimize the leakage signals.

Assuming that the phase of the leakage signal collected in advance and the phase of the leakage signal during the operation of the radar sensor are different from each other, the signal after leakage subtraction can be expressed as follows:

$$\begin{aligned} &y(t)-y_{leakage\ saved}\text{''}(t)= \\ &\underbrace{A_{leakage}(t)\cos(2\pi k\tau_{leakage}t+\theta_2)}_{leakage\ signal} \\ &\quad+\underbrace{A_{target}(t)\cos\left(2\pi k\tau_{target}t+\theta_3+\varphi_1(t)-\varphi_3(t)\right)}_{target\ signal} \\ &\quad-\underbrace{A_{leakage}\text{''}(t)\cos(2\pi k\tau_{leakage}t+\theta_2\text{''})}_{leakage\ saved\ in\ advance} \end{aligned} \tag{8}$$

Because a coherent miniaturized radar sensor can produce every chirp signal with consistent characteristics, the amplitudes of the leakage signals are almost identical. Thus, the expression can be written as below:

$$A_{leakage}(t)\cong A_{leakage}\text{''}(t) \tag{9}$$

$$\theta_2\text{''}=\theta_2+\Delta\ (\ phase\ difference\ ) \tag{10}$$

$$\begin{aligned} &y(t)-y_{leakage\ saved}\text{''}(t) \\ &\cong\underbrace{A_{leakage}(t)\left(\cos(2\pi k\tau_{leakage}t+\theta_2)-\cos(2\pi k\tau_{leakage}t+\theta_2+\Delta)\right)}_{leakage\ substraction} \\ &\quad+\underbrace{A_{target}(t)\cos(2\pi k\tau_{target}t+\overbrace{\theta_3+\varphi_1(t)-\varphi_3(t)}^{\varphi(t)})}_{target\ signal} \end{aligned} \tag{11}$$

D. Phase-Synchronized Leakage Subtraction Considering IQ Imbalance Factor

The process in the receiver of a homodyne radar sensor typically uses an RC polyphase filter to down-convert the RF signal to the baseband in the analog domain. However, down-conversion with an RC polyphase filter results in amplitude and phase imbalances. These imbalances are caused by factors such as asymmetry in the phase paths within the filter, differential length between the signal paths, and phase noise in the reference chirp signal. Because amplitude and phase imbalances occur between I and Q channels, we will prove the validity of the proposed method by considering these factors in the mathematical expression. In radar operation, subtraction of the pre-stored leakage signal data from the received signal data is done by the DSP. Therefore, we can express the leakage subtraction process considering the amplitude imbalance factor (α) and the phase imbalance factor (β) as the formula shown below:

$$\begin{aligned} &y[n]-y_{leakage\ saved}\text{''}[n] \\ &=\underbrace{A_{leakage}[n]\left(\cos[2\pi k\tau_{leakage}n+\theta_2]+j\alpha\sin[2\pi k\tau_{leakage}n+\theta_2+\beta]\right)}_{leakage\ signal} \\ &+\underbrace{A_{target}[n]\left(\cos[2\pi k\tau_{target}n+\varphi(t)]+j\alpha\sin[2\pi k\tau_{target}n+\varphi(t)+\beta]\right)}_{target\ signal} \\ &\underbrace{-A_{leakage}\text{''}[n]\left(\cos[2\pi k\tau_{leakage}n+\theta_2+\Delta]+j\alpha\sin[2\pi k\tau_{leakage}n+\theta_2+\Delta+\beta]\right)}_{leakage\ saved\ in\ advance} \end{aligned} \tag{12}$$

If the subtraction operation is performed only with the time synchronization without considering the phase difference, it does not significantly reduce the amplitude of the leakage signal because of the phase difference. Therefore, we mathematically analyze whether the amplitude of the leakage signal can be further reduced by adjusting the phase-synchronized leakage subtraction through the multiplication operation of $exp(j\phi)$ with the pre-stored leakage data. A block diagram of the phase synchronization

process between leakage signals is shown in Fig.8. To simplify the formula, we express it as follows:

$$2\pi k\tau_{leakage}n+\theta_2=A \tag{13}$$

$$2\pi k\tau_{target}n+\varphi(t)=B \tag{14}$$

$$\begin{aligned} &y[n]-y_{leakage\ saved}"[n]\times exp(j\phi)\\ &=\underbrace{A_{leakage}[n]\left(\cos[A]+j\alpha\sin[A+\beta]\right)}_{leakage\ signal}\\ &\quad-\underbrace{A_{leakage}"[n]\left(\cos[A+\Delta]+j\alpha\sin[A+\Delta+\beta]\right)\times exp(j\phi)}_{leakage\ saved\ and\ phase\ synchronization}\\ &\quad+\underbrace{A_{target}[n]\left(\cos[B]+j\alpha\sin[B+\beta]\right)}_{target\ signal} \end{aligned} \tag{15}$$

To calculate the phase synchronization term ϕ in (15), we propose a method for determining the relative phase value between the baseband signals and the pre-stored leakage. We apply the FFT to $y[n]$ and $y_{leakage\ saved}"[n]$, and then transform these results into frequency domain and phase response. Subsequently, the phase response value of the leakage signal could be identified by finding the maximum value within the frequency domain. This approach is effective because of the substantial power of the leakage signal compared to that of the target signal. To minimize errors caused by inadequate frequency domain resolution, zero-padding is used before applying the FFT. This enables accurate identification of the signal peak in the frequency domain. This technique facilitates the extraction of the index number corresponding to the peak power, which is necessary for calculating the phase difference between $y[n]$ and $y_{leakage\ saved}"[n]$. To achieve phase-synchronized leakage mitigation, $y_{leakage\ saved}"[n]$ is multiplied by exp(jϕ), where ϕ represents the calculated phase difference. Therefore, as shown in Fig.8, there are 4 steps for implementing phase synchronized leakage subtraction.

1) FFT analysis: applying FFT to the IQ data of $y[n]$ and $y_{leakage\ saved}"[n]$, transforming into the frequency domain.

2) Phase extraction: extracting the phase value corresponding to leakage signal.

$$k_{leakage}=\arg\max\left|Y[k]\right|^2 \tag{16}$$

$$phase\ of\ leakage=\angle Y[k_{leakage}] \tag{17}$$

3) Phase difference (ϕ) calculation: determining the phase synchronization term ϕ by calculating the phase difference between $y[n]$ and $y_{leakage\ saved}"[n]$.

$$phase\ difference=\angle Y_1[k_{leakage}]-\angle Y_2[k_{leakage}] \tag{18}$$

Where $Y_1[k]$, $Y_2[k]$ is the result of N-point FFT of $y[n]$ and $y_{leakage\ saved}"[n]$. $\angle Y$ is the phase response of $Y[k]$. The phase

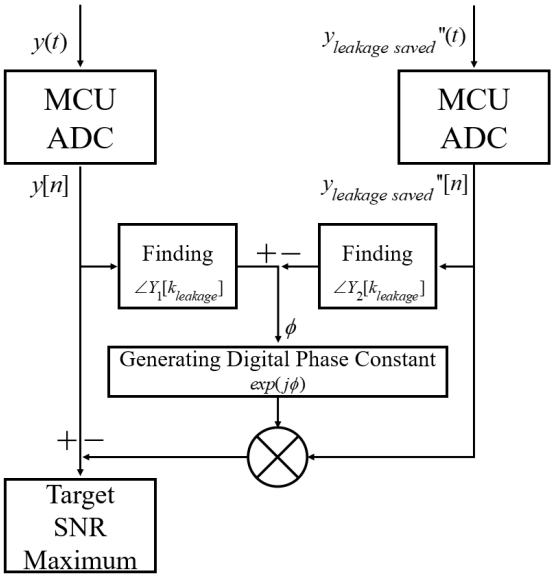

Fig. 8. Block diagram of the phase synchronization process for miniaturized FMCW radar.

difference between $y[n]$ and $y_{leakage\ saved}"[n]$ is known from (18). The synchronized phase can be estimated as:

$$\phi\cong\angle Y_1[k_{leakage}]-\angle Y_2[k_{leakage}] \tag{19}$$

4) Phase-synchronized leakage subtraction: implementing the mathematical expression in (15).

Then, the phase synchronized leakage is expressed as $y_{leakage\ saved}"[n]\times exp(j\phi)$. Considering the consistent characteristics of the coherent FMCW radar sensor, the amplitudes of the leakage signal data are almost similar. The result of the subtraction between the leakage signal data and the phase-synchronized leakage data is as follows:

$$A_{leakage}(n)\cong A_{leakage}"(n) \tag{20}$$

$$\angle Y_1[k_{leakage}]-\angle Y_2[k_{leakage}]\cong-\Delta \tag{21}$$

$$\begin{aligned} &y[n]-y_{leakage\ saved}"[n]\times exp(j\phi)\\ &=A_{leakage}[n]\Big(\cancel{\cos[A]+j\sin[A]}+j\sin[A](\alpha\cos\beta-1)\\ &\qquad+j\alpha\cos[A]\sin\beta\Big)\\ &-A_{leakage}"[n]\Big(\cancel{\cos[A+\Delta]+j\sin[A+\Delta]}\\ &\qquad+j\sin[A+\Delta](\alpha\cos\beta-1)\\ &\qquad+j\alpha\cos[A+\Delta]\sin\beta\Big)\times\underbrace{\exp(-j\Delta)}_{phase\ synchronized}\\ &\qquad+\underbrace{A_{target}[n]\left(\cos[B]+j\alpha\sin[B+\beta]\right)}_{target\ signal}\\ &\cong A_{leakage}[n]\left(j\sin[A](\alpha\cos\beta-1)\right) \end{aligned}$$

$$+ j\alpha\cos[A]\sin\beta - \exp(-j\Delta)\, j\sin[A+\Delta](\alpha\cos\beta - 1) - \exp(-j\Delta)\, j\alpha\cos[A+\Delta]\sin\beta \Big)}_{\text{remaining leakage components}} + \underbrace{A_{target}[n]\big(\cos[B] + j\alpha\sin[B+\beta]\big)}_{\text{target signal}} \quad (22)$$

We simplify the mathematical description by focusing mainly on the analysis of the leakage signal data characterized by their main beat frequency components, namely $\sin[A]$ and $\cos[A]$. To achieve this, we have performed a comprehensive mathematical extension including complex exponential and trigonometric functions. This process allowed a more in-depth analysis of the effects on the amplitude of the leakage signal data by integrating the results into expressions involving $\sin[A]$ and $\cos[A]$.

$$\therefore \quad y[n] - y_{leakage\ saved}\text{"}[n] \times \underbrace{exp(-j\Delta)}_{\text{phase synchroized}}$$

$$\cong \underbrace{\sin\Delta}_{<1} \times A_{leakage}[n]\Big(\sin[A]\{\alpha\sin\beta\sin\Delta + (1-\alpha\cos\beta)\cos\Delta\} + \cos[A]\{(1-\alpha\cos\beta)\sin\Delta - \alpha\sin\beta\cos\Delta\} + j\sin[A]\{\alpha\sin\beta\cos\Delta - \sin\Delta(1-\alpha\cos\beta)\} + j\cos[A]\{\alpha\sin\beta\sin\Delta + \sin\Delta(1-\alpha\cos\beta)\}\Big)}_{\text{remaining leakage components}} + \underbrace{A_{target}[n]\big(\cos[B+\varphi(t)] + j\alpha\sin[B+\varphi(t)+\beta]\big)}_{\text{target signal}} \quad (23)$$

Mathematical analysis shows that after subtracting the phase-synchronized leakage signal data, the remaining components are composed of the amplitude and phase imbalance factor. Given that the $\sin(\Delta)$ term is less than one and the IQ imbalance factor is also small [30]-[32], the amplitude of the leakage signal is significantly diminished. The mathematical analysis proved that the phase-synchronized leakage subtraction can significantly reduce the original leakage signal amplitude. Therefore, we mathematically verify that the time- and phase-synchronized leakage subtraction method can effectively reduce leakage signal power with the target power unchanged.

IV. Fabrication and Experiment Setup

As shown in Fig. 9, we fabricated a miniaturized FMCW radar sensor (diameter 35 mm). To make it small, we used a multi-layer design, integrating circuits with different functions on each layer, and constructed the system with two functionally different boards. The specifications of the fabricated radar sensor are detailed in Table 2. To verify the operation of the miniaturized radar sensor, the control mechanism was measured using a logic analyzer (16702B). This procedure is essential to verify the control functionality of the sensors in accordance with the synchronized approach proposed in Section III. The measurement results from the logic analyzer showed that after the transceiver enable signal is activated, the MCU gives a start trigger to the PLL. Subsequently, the PLL sends control signals to the MCU for ADC sampling and the transceiver for K-band signal radiation simultaneously. The measurement results shown in Fig. 10(b) confirm that the control mechanism functions correctly as proposed in Fig. 7(b).

TABLE II
Parameters of Homodyne FMCW Radar Sensor for Experiment

Parameters	Values
Operating frequency	24.45-24.75 GHz
Transmit power	23 dBm
Antenna gain	11.56 dBi
Sweep bandwidth	300 MHz
Range resolution	0.5 m
Chirp duration	500 us
# of samples in a chirp	256
NFFT	1024
Chirp type	Triangular

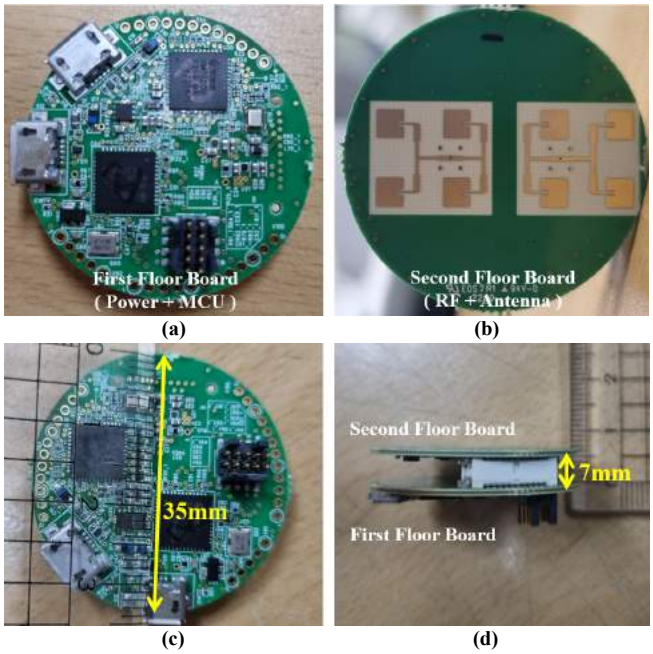

Fig. 9. Picture of manufactured K-band homodyne FMCW radar (a) Bottom view of the first-floor board. (b) Top view of the second-floor board. (c) Bottom view of the K-band homodyne FMCW radar. (d) Side view of the K-band homodyne FMCW radar.

We conducted three different experiments at the playground of the KAIST mun-ji campus to validate the proposed method in Section III to mitigate increased leakage signals in the miniaturized radar sensor. In Experiment A, the antennas of the radar sensor were pointed at the sky to collect the leakage IQ data of the FMCW sensor as shown in Fig. 11(a). This experiment facilitates the analysis of the baseband IQ signal for each chirp. We examined the coherence and amplitude variation in leakage IQ signals generated by the chirps. In addition, the leakage IQ data were collected at different times to ascertain the phase difference. We also focused on how much the proposed method can reduce the power of leakage signals without a target. Experiments B and C are conducted with a target to see how much the power of the leakage signal can be attenuated. In Experiment B, we flew a drone (DJI Inspire2)

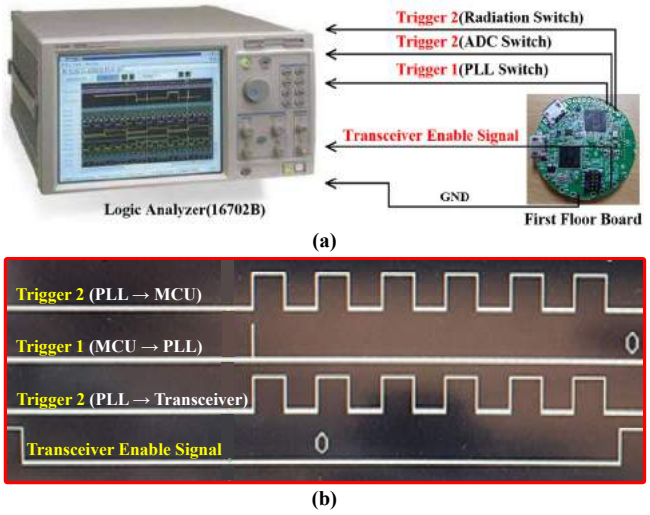

Fig. 10. Measurement of radar sensor control mechanism. (a) Logic analyzer measurement setup with fabricated first-floor board. (b) Logic analyzer results.

with low reflectivity ($RCS \ \ 0.01m^2$) while the antennas of the radar sensor pointed to the sky as shown in Fig. 11(b). Experiment B is conducted to assess the effectiveness of the proposed method in detecting targets with low reflectivity. In Experiment C, we focused on the practical applicability of the

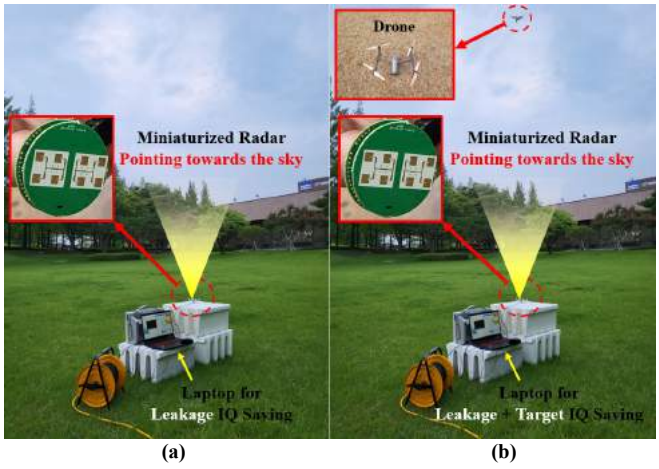

Fig. 11. Radar sensor experiment setup at KAIST Mun-ji Campus. (a) Experiment A with no targets. (b) Experiment B with a drone (DJI Inspire2.)

Fig. 12. Radar sensor experiment setup at KAIST Mun-ji Campus. (a) Experiment C setup. (b) Experiment C with targets.

sensor when the antennas of the radar sensor radiate radio waves horizontally parallel to the ground as shown in Fig. 12. Experiment C is conducted to investigate how the proposed method contributes to enhancing radar sensor sensitivity.

V. Measured Results and Discussion

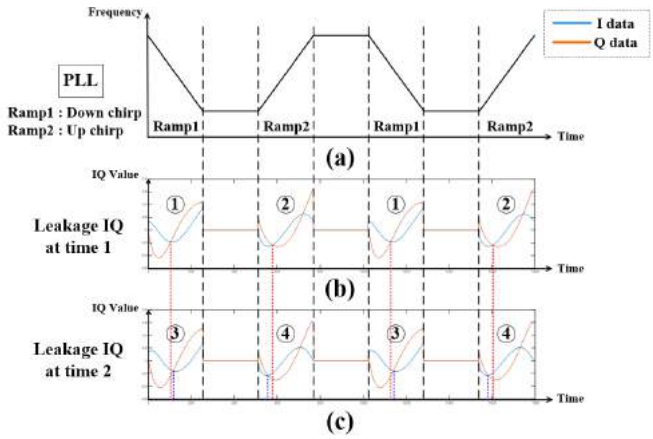

Fig. 13. Measurement of leakage IQ signal at different times in Experiment A. (a) Frequency of transmitted ramp chirps as a function of time. (b) The resulting leakage IQ data at time 1 as a function of time. (c) The resulting leakage IQ data at time 2 as a function of time.

Fig. 13 presents the leakage IQ signal obtained from Experiment A. Fig. 13(a) illustrates the chirp signal in the miniaturized FMCW homodyne radar sensor, explaining the linear frequency decrease and increase in the time domain. Fig. 13(b) corresponds to the resulting leakage IQ signal data in the time domain at time 1. Fig. 13(c) corresponds to the resulting leakage IQ signal data in the time domain at time 2. Unlike the IQ in Fig. 5(b), the leakage IQ signal were coherent for each chirp. At time 1, the leakage IQ signal remained coherent when the chirp slope was the same. After turning off the power and resuming the experiment, the leakage IQ signal at time 2 was also confirmed to be coherent between chirps with the same slope. These results demonstrate that our miniaturized radar sensor, designed with a frequency sweep plan to minimize baseband noise and equipped with a synchronized control mechanism in the MCU, successfully achieves a coherent baseband signal. However, when comparing the leakage IQ signal at different times (Time 1 and Time 2), there is a difference between the leakage IQ signal, even those generated by the same chirp. The crossing points of the I and Q values, indicated by the red and blue dots, occur at different points. This variation in the crossing points is due to the phase difference between the time 1 and time 2 leakage IQ signal. These phase differences are caused by turning power on and off in the FMCW radar sensor.

To address the phase synchronization of leakage signals in a miniaturized FMCW radar sensor, our study introduces an approach to calculate the phase difference directly from the frequency domain characteristics of the signals, as shown in section III-D. Based on this method, the phase difference values between the leakage signals in Experiments A, B, and C are calculated and presented in Table 3. By applying the proposed

TABLE III
PHASE DIFFERENCE VALUE FOR PHASE SYNCHRONIZATION

Experiment	Parameters	Values
A	Up chirp angle difference	13.37°
A	Down chirp angle difference	13.96°
B	Up chirp angle difference	-8.34°
B	Down chirp angle difference	-8.77°
C	Up chirp angle difference	-8.84°
C	Down chirp angle difference	-8.86°

method, we found out how much the power of the leakage signal can be attenuated compared to leakage signal power before subtraction. 0° phase synchronization subtraction means the time-synchronized leakage subtraction. Fig. 14 presents the results obtained from Experiment A. Fig. 14(a), (b), and (c) show the results obtained by the radar sensor during the emission of an up chirp, while Fig. 14(d), (e), and (f) show the results corresponding to the emission of a down chirp. Fig. 14(a) and (d) illustrate the impact of the ϕ values used in the phase adjustment on the power of the leakage signal at time 1 after the subtraction operation. The blue line in Fig. 14(a) and (d) represents the residual power of the leakage signal after subtraction leakage signal at time 2 multiplied by a series of $exp(j\phi)$ from leakage signal at time 1. These exponential factors were implemented in 0.5° increments, covering a range from -45°(-π/4) to 45°(π/4). To verify the phase synchronization term in Table 3 obtained from the method in section III-D, the phase synchronization term is indicated by a red point in Fig. 14(a) and (d). Fig. 14(a) and (d) indicate that the 13.5° and 14° phase exponential constants are needed for phase synchronization between leakage signals in Experiment A. This red point closely approximates the point that yields the lowest residual leakage power, confirming the precision of the synchronization term. Also, this minimum leakage power confirms the need for phase synchronization in the leakage subtraction process. Fig. 14(b) and (e) provide a comparative analysis of power spectra after three different results: the leakage signal before subtraction, applying time-synchronized leakage subtraction, and applying proposed leakage subtraction. We observed a significant reduction in leakage signal power following the application of our proposed method. Specifically, the power reduction for the leakage signal in the up chirp is approximately 33 dB, while in the down chirp, it is around 31 dB. Fig. 14(c) and (f) show the comparative noise improvement, showing the difference between the power spectra of the leakage signal after time-synchronized leakage subtraction and proposed leakage subtraction. This comparison is made by subtracting the aligned power spectra shown in Fig. 14(b) and (e). After subtracting the aligned power spectra, as shown in Fig. 14(b) and (e), the resulting data were processed through a fourth-order curve fitting function. Subsequently, the magnitude of the noise improvement for the up chirp ranged from 9 to 13.5 dB, and for the down chirp it ranged from 6 to 9 dB. In summary, Fig. 14 demonstrates the effectiveness of our

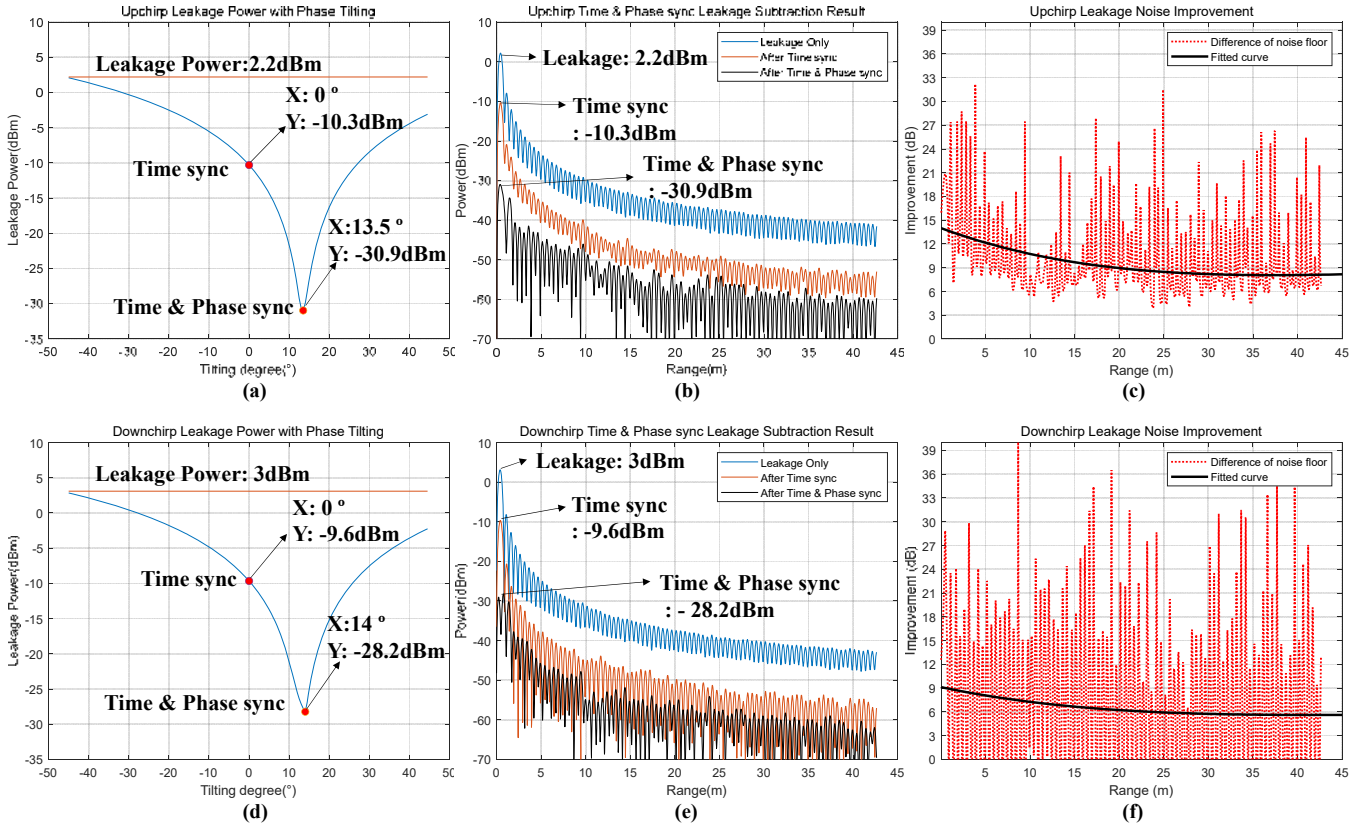

Fig. 14. Results of Experiment A. (a) and (d) Variation of leakage power after subtraction of leakage signal multiplied by exp(jØ). (b) and (e) Power spectra comparison: Only leakage, time-sync leakage subtraction method, and proposed method. (c) and (f) Noise improvement: Power spectra difference between time-synchronized and proposed method in Experiment A.

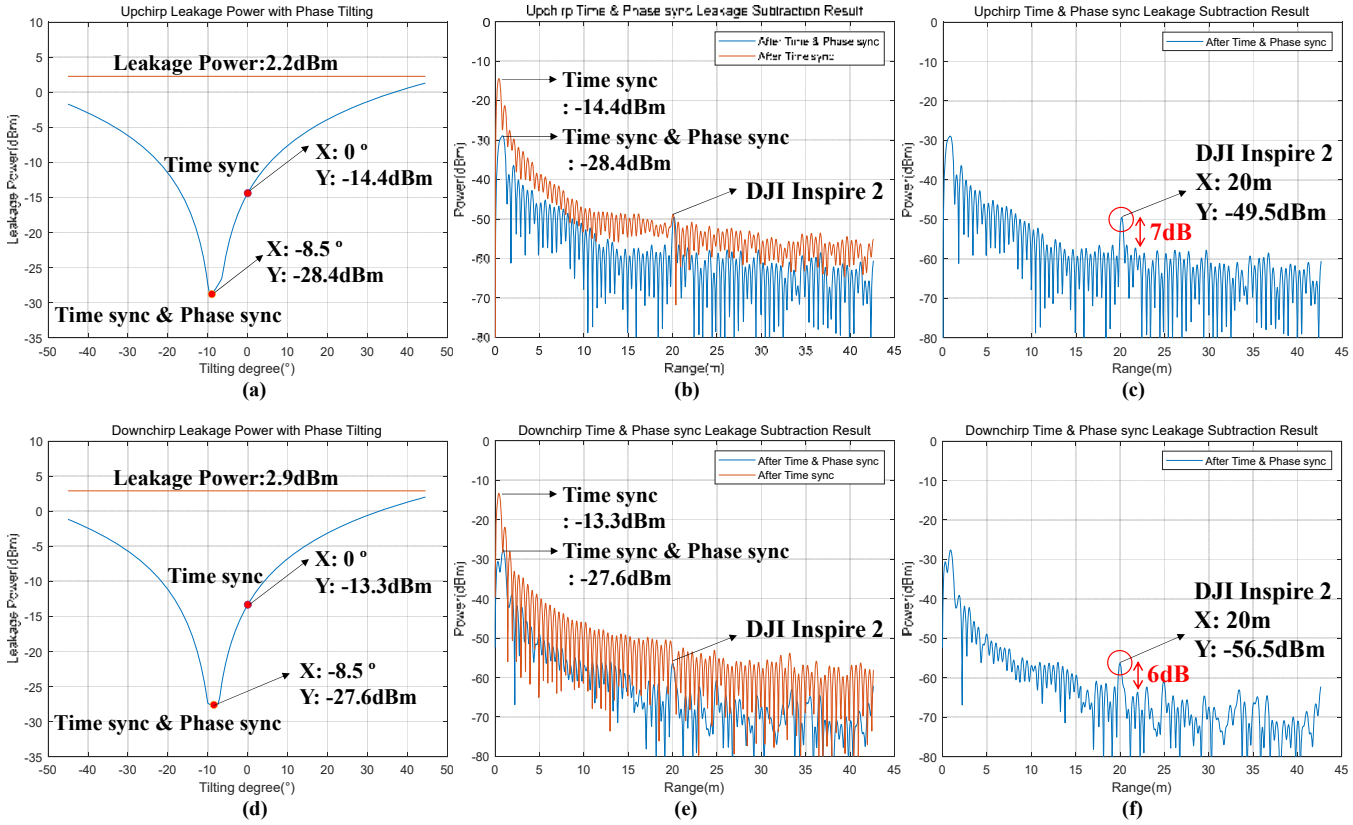

Fig. 15. Results of Experiment B. (a) and (d) Variation of leakage power after subtraction of leakage signal multiplied by exp(jØ). (b) and (e) Performance comparison of the power spectra between time sync and the proposed method. (c) and (f) Power spectra from proposed method.

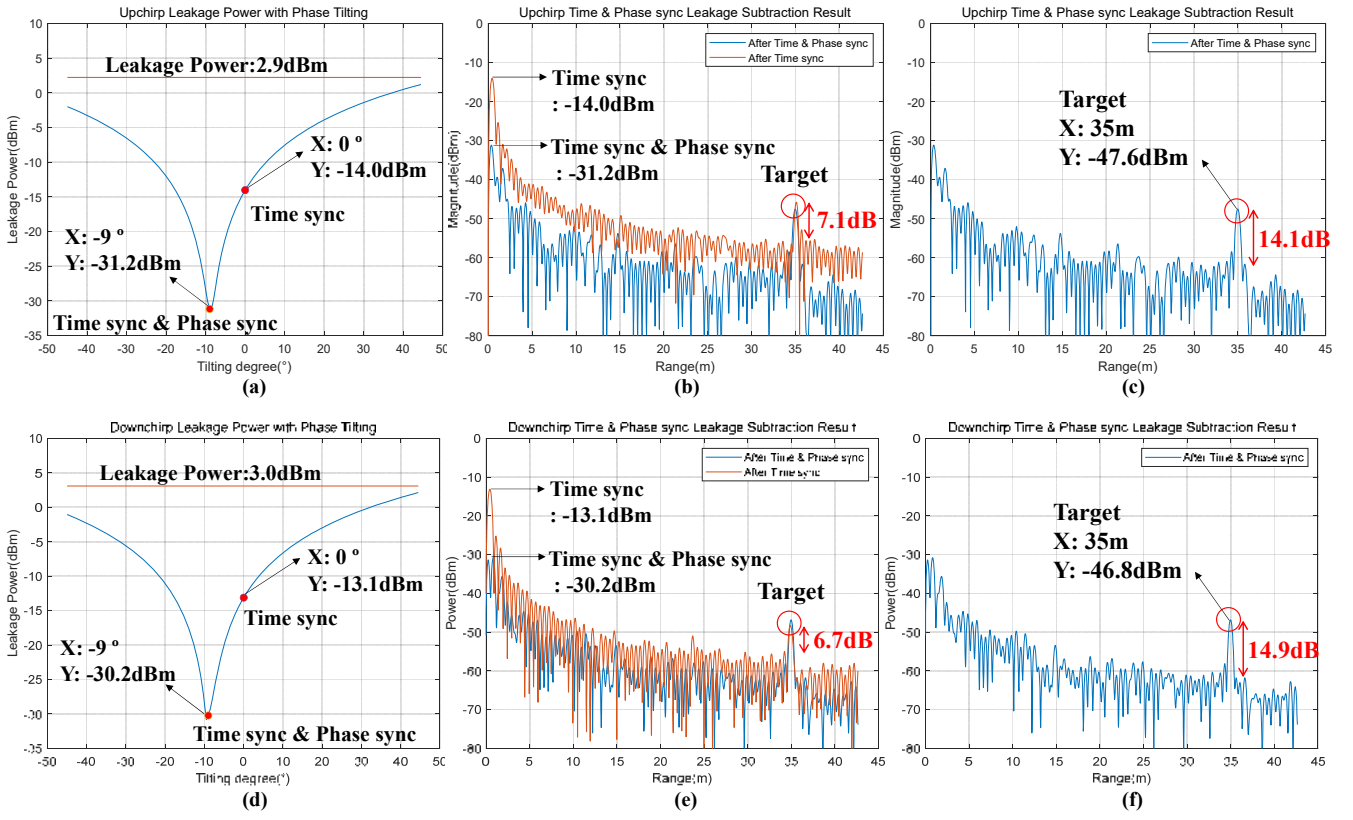

Fig. 16. Results of Experiment C. (a) and (d) Variation of leakage power after subtraction of leakage signal multiplied by exp(jØ). (b) and (e) Performance comparison of the power spectra between time sync and proposed method. (c) and (f) Power spectra from proposed method.

proposed method in reducing the leakage signal power and the associated noise floor.

In Experiment B, a triangular chirp was used to detect a drone (DJI Inspire2) with a small RCS at a distance of 20 m. The distance between the radar sensor and the drone was accurately ascertained using GPS data in the remote control. Fig. 15 presents the results obtained from Experiment B. Fig. 15(a), (b), and (c) show the results obtained by the radar sensor during the emission of an up chirp, while Fig. 15(d), (e), and (f) show the results corresponding to the emission of a down chirp. Fig. 15(a) and (d) indicate that the -8.5° phase exponential constant is needed for phase synchronization between leakage signals in Experiment B. As shown in Fig. 15(b) and (e), the drone was not detected using only time-synchronized leakage subtraction because of low RCS. However, improved SNR was achieved after time- and phase-synchronized leakage subtraction. As demonstrated in Fig. 15(c) and (f), the implementation of our approach showed an improvement in SNR of about 7 dB in the up chirp and about 6 dB in the down chirp. In addition, our proposed method attenuates the power of leakage signals by about 17 dB rather than time-synchronized leakage subtraction, effectively reducing the overall noise floor and increasing the SNR. Therefore, the drone was successfully detected after applying our proposed method, which combines phase-synchronized leakage subtraction operation.

In Experiment C, we put the antenna of the radar sensor horizontally to the ground for industrial application. Fig. 16 presents the results obtained from Experiment C. Fig. 16(a), (b), and (c) show the results obtained by the radar sensor during the emission of an up chirp, while Fig. 16(d), (e), and (f) show the results corresponding to the emission of a down chirp. Fig. 16(a) and (d) indicate that the -8.5° and -9° phase exponential constants are needed for phase synchronization between leakage signals in Experiment C. The results in Fig. 16(b) and (e) show that targets with greater RCS than drones can be detected using only time-synchronized leakage subtraction because of their high RCS. However, time- and phase-synchronized leakage subtraction allows the target power to remain nearly constant while reducing the noise around the target range bin. Specifically, the SNR for a target at 35 m is improved by approximately 7 dB for the up chirp, from 7.13 dB to 14.18 dB, and by approximately 8.1 dB for the down chirp, from 6.77 dB to 14.9 dB, as demonstrated in Fig. 16(c) and (f). In addition, the leakage signal power was attenuated by about 17 dB for the up chirp and 17.7 dB for the down chirp compared to the leakage signal power after the time-synchronized leakage subtraction. Therefore, it was verified that the sensitivity of the radar sensor can be increased by the proposed method.

VI. Comparisons with Other Works

Table IV compares the proposed method with other recent leakage mitigation methods. The method presented in [15]-[16] is designed to reduce the phase noise of leakage signals generated from heterodyne FMCW radar sensors. Unlike [15]-[16], the baseband signal of the homodyne FMCW radar sensor has minimal phase noise because of the range correlation effect. The method proposed in [17] is time-synchronized leakage subtraction by iterative comparison. However, due to the significant computational demands, this approach may not be practical in real applications. Also, additional hardware other than radar is needed to implement the method proposed in [17]. In [25]-[26], a signal that is similar to the leakage signal must be additionally inserted into the chip by implementing a delay line in the circuit to subtract a leakage signal. This method also needs an additional delay line within the circuit. In

TABLE IV
Comparison Between Proposed Method and Other Method in Leakage Mitigation

Paper	Method	System size	Requirement of additional hardware	Leakage mitigation	Noise Improvement
[15]-[16]	Concentrating the phase noise of the leakage signal on its stationary point.	Bulky	Not required	30 dB	7~10 dB
[17]	The time synchronization subtract process through two distinct iterations following the advance save of the leakage signal.	Bulky	required	35.5~38.5 dB	5~10 dB
[25]-[26]	Utilizing an artificial on-chip target(OCT), which makes use of delay line within the circuit	Bulky	required	-	5 dB
Proposed	The time and phase synchronization subtract process without iterations following the advance save of the leakage signal.	35 mm x 35 mm	Not required	31~33 dB	6~9 dB

order to specify the delay of the generated leakage signal, complex calculation processes such as cross-correlation or mean square error estimator are required. In contrast, we introduced a highly sophisticated control mechanism to adjust the time synchronization between signals before proceeding with leakage subtraction. Also, the proposed phase synchronization method through relatively simple FFT analysis adjusts the phase difference between leakage signals. The phase difference between leakage signals can occur due to changes in temperature or voltage and can vary due to phase noise. Our method achieves leakage signal mitigation through software and signal processing without the need for additional hardware.

VII. Conclusion

We have explained and demonstrated the time- and phase-synchronized leakage subtraction method, a novel approach to mitigate dominant leakage in miniaturized homodyne FMCW radar sensors. This study effectively addresses the variations in the phase of the leakage signal. Additionally, the paper verifies the solutions to phase variation mathematically and experimentally. On the basis of theory and experiments, we have confirmed that this method can effectively mitigate the leakage signal power, thereby increasing the sensitivity of radar sensors without the need for additional hardware. In conjunction with the proposed method, integrating advanced signal processing techniques such as adaptive filtering can be highly effective. Also, the proposed method can be applied to both heterodyne and homodyne radar architectures because most signals in these systems manifest as sinusoidal forms. Additionally, we measured the time required for phase synchronized leakage subtraction. Matlab was used with the tic-toc function to measure the required time. The result was approximately 0.056 seconds. This indicates that our method can be implemented in real-time using a standard MCU with the operational speeds required for robust radar applications.

The proposed method can enhance the utility of miniaturized FMCW radar sensors across various industries, including robotics and automotive. There are challenges for miniaturized FMCW radar sensors in various industries. The radar sensor must process the captured signals in real-time to ensure immediate responsiveness, which is critical in applications such as autonomous driving and robotic navigation. Because the MCU chip controls the radar and processes the captured signals simultaneously, the MCU needs to allocate the operational time according to the specific requirements of each role. Due to the limited time available for signal processing, reducing computational complexity is important. Our proposed method, which employs FFT analysis, allows for faster computational speeds. Consequently, this enables FMCW radar sensors to be utilized across various industries. In addition, commercialized small-sized FMCW radars must overcome the challenge of detecting objects at close range, given that most radar sensor commercialization is based on short-range detection [6]-[8], [11]-[13]. From this perspective, we have fabricated miniaturized FMCW radar sensors, including antennas, and successfully mitigated the leakage signal problems through signal processing solutions considering the random characteristics of leakage signals. In practical applications, radar sensors are frequently subjected to power cycling and temperature variations, causing random characteristics to leakage signals. Despite these random variations, our proposed signal processing method effectively maximizes the mitigation of leakage signals. This will increase their applicability in various industries.

References

[1] E. Tavanti, A. Rizik, A. Fedeli, D. D. Caviglia and A. Randazzo, "A Short-Range FMCW Radar-Based Approach for Multi-Target Human-Vehicle Detection," in IEEE Transactions on Geoscience and Remote Sensing, vol. 60, pp. 1-16, 2022.

[2] D. K. A. Pulutan and J. S. Marciano, "Design trade-offs in a combined FMCW and pulse Doppler radar front-end," IEEE 2013 Tencon - Spring, Sydney, NSW, Australia, 2013, pp. 567-571.

[3] E. L. Christensen, S. N. Madsen and N. Skou, "Review of the homodyne technique for coherent radar," IEEE International Conference on Radar, Arlington, VA, USA, 1990, pp. 159-163.

[4] B. Razavi, "Design considerations for direct-conversion receivers," in IEEE Transactions on Circuits and Systems II: Analog and Digital Signal Processing, vol. 44, no. 6, pp. 428-435, June 1997.

[5] C. Li et al., "A Review on Recent Progress of Portable Short-Range Noncontact Microwave Radar Systems," in IEEE Transactions on Microwave Theory and Techniques, vol. 65, no. 5, pp. 1692-1706, May 2017.

[6] C. Will, P. Vaishnav, A. Chakraborty and A. Santra, "Human Target Detection, Tracking, and Classification Using 24-GHz FMCW Radar," in IEEE Sensors Journal, vol. 19, no. 17, pp. 7283-7299, 1 Sept.1, 2019.

[7] P. Withington, H. Fluhler and S. Nag, "Enhancing homeland security with advanced UWB sensors," in IEEE Microwave Magazine, vol. 4, no. 3, pp. 51-58, Sept. 2003.

[8] J. M. Munoz-Ferreras, F. Perez-Martinez, J. Calvo-Gallego, A. Asensio-Lopez, B. P. Dorta-Naranjo and A. Blanco-del-Campo, "Traffic Surveillance System Based on a High-Resolution Radar," in IEEE Transactions on Geoscience and Remote Sensing, vol. 46, no. 6, pp. 1624-1633, June 2008.

[9] H. Wang et al., "SleepSense: Smart Pillow With Pressure-Sensitive FBG-Embedded Silicone Buttons," in IEEE Sensors Journal, vol. 23, no. 17, pp. 19324-19331, 1 Sept.1, 2023.

[10] W. Zhang, R. Singh, F. -Z. Liu, C. Marques, B. Zhang and S. Kumar, "WaveFlex Biosensor: A Flexible-Shaped Plasmonic Optical Fiber Sensor for Histamine Detection," in IEEE Sensors Journal, vol. 23, no. 19, pp. 22533-22542, 1 Oct.1, 2023.

[11] Ding, Chuanwei & Hong, Hong & Zou, Yu & Chu, Hui & Zhu, Xiaohua & Fioranelli, Francesco & le kernec, Julien & Li, Changzhi. (2019). Continuous Human Motion Recognition With a Dynamic Range-Doppler Trajectory Method Based on FMCW Radar. IEEE Transactions on Geoscience and Remote Sensing. PP. 10.1109/TGRS.2019.2908758.

[12] A. D. Droitcour, O. Boric-Lubecke, V. M. Lubecke, J. Lin and G. T. A. Kovacs, "Range correlation and I/Q performance benefits in single-chip silicon Doppler radars for noncontact cardiopulmonary monitoring," in IEEE Transactions on Microwave Theory and Techniques, vol. 52, no. 3, pp. 838-848, March 2004.

[13] B. -K. Park, O. Boric-Lubecke and V. M. Lubecke, "Arctangent Demodulation With DC Offset Compensation in Quadrature Doppler Radar Receiver Systems," in IEEE Transactions on Microwave Theory and Techniques, vol. 55, no. 5, pp. 1073-1079, May 2007

[14] Biswas, A., & Wang, H. (2022). Autonomous Vehicles Enabled by the Integration of IoT, Edge Intelligence, 5G, and Blockchain. *Sensors*, *23*(4), 1963.

[15] J. Park, S. Park, D. -H. Kim and S. -O. Park, "Leakage Mitigation in Heterodyne FMCW Radar for Small Drone Detection With Stationary Point Concentration Technique," in IEEE Transactions on Microwave Theory and Techniques, vol. 67, no. 3, pp. 1221-1232, March 2019.

[16] J. Park, J. -S. Park, K. -B. Bae and S. -O. Park, "Advanced Stationary Point Concentration Technique for Leakage Mitigation and Small Drone Detection With FMCW Radar," in IEEE Transactions on Microwave Theory and Techniques, vol. 69, no. 3, pp. 1791-1804, March 2021.

[17] J. Liu, J. Lu, Y. Li, C. Gu and J. Mao, "Mitigation of Leakage and Stationary Clutters in Short-Range FMCW Radar With Hybrid Analog and Digital Compensation Technique," in IEEE Transactions on Microwave Theory and Techniques, vol. 70, no. 1, pp. 62-73, Jan. 2022.
[18] D. -H. Shin, D. -H. Jung, D. -C. Kim, J. -W. Ham and S. -O. Park, "A Distributed FMCW Radar System Based on Fiber-Optic Links for Small Drone Detection," in IEEE Transactions on Instrumentation and Measurement, vol. 66, no. 2, pp. 340-347, Feb. 2017.
[19] J. -S. Suh, L. Minz, D. -H. Jung, H. -S. Kang, J. -W. Ham and S. -O. Park, "Drone-Based External Calibration of a Fully Synchronized Ku-Band Heterodyne FMCW Radar," in IEEE Transactions on Instrumentation and Measurement, vol. 66, no. 8, pp. 2189-2197, Aug. 2017.
[20] K.-B. Kong, W.-R. Jeong, and S.-O. Park, "Design and initial measurements of K-band FMCW rain radar with high resolution," Microw. Opt. Technol. Lett., vol. 58, no. 4, pp. 817–822, Apr. 2016.
[21] P. D. L. Beasley, A. G. Stove, B. J. Reits and B. As, "Solving the problems of a single antenna frequency modulated CW radar," IEEE International Conference on Radar, Arlington, VA, USA, 1990, pp. 391-395.
[22] K. Lin, Y. E. Wang, C. -K. Pao and Y. -C. Shih, "A Ka-Band FMCW Radar Front-End With Adaptive Leakage Cancellation," in IEEE Transactions on Microwave Theory and Techniques, vol. 54, no. 12, pp. 4041-4048, Dec. 2006.
[23] J.-G. Kim, Sangsoo Ko, Sanghoon Jeon, Jae-Woo Park and Songcheol Hong, "Balanced topology to cancel Tx leakage in CW radar," in IEEE Microwave and Wireless Components Letters, vol. 14, no. 9, pp. 443-445, Sept. 2004.
[24] C. -Y. Kim, J. -G. Kim and S. Hong, "A Quadrature Radar Topology With Tx Leakage Canceller for 24-GHz Radar Applications," in IEEE Transactions on Microwave Theory and Techniques, vol. 55, no. 7, pp. 1438-1444, July 2007.
[25] A. Melzer, F. Starzer, H. Jäger and M. Huemer, "Real-Time Mitigation of Short-Range Leakage in Automotive FMCW Radar Transceivers," in IEEE Transactions on Circuits and Systems II: Express Briefs, vol. 64, no. 7, pp. 847-851, July 2017.
[26] A. Melzer, M. Huemer and A. Onic, "Novel mixed-signal based short-range leakage canceler for FMCW radar transceiver MMICs," 2017 IEEE International Symposium on Circuits and Systems (ISCAS), Baltimore, MD, USA, 2017, pp. 1-4.
[27] S. Häfner, A. Dürr, C. Waldschmidt and R. Thomä, "Mitigation of Leakage in FMCW Radars by Background Subtraction and Whitening," in IEEE Microwave and Wireless Components Letters, vol. 30, no. 11, pp. 1105-1107, Nov. 2020.
[28] W. Wang et al., "Wideband Gain Enhancement of MIMO Antenna and Its Application in FMCW Radar Sensor Integrated With CMOS-Based Transceiver Chip for Human Respiratory Monitoring," in IEEE Transactions on Antennas and Propagation, vol. 71, no. 1, pp. 318-329, Jan. 2023.
[29] J. Han and R. Chen, "Research of a Miniaturized Broadband Mems Phase Detector and its Temperature Effect for Application in Phase-Locked Loops," 2019 20th International Conference on Solid-State Sensors, Actuators and Microsystems & Eurosensors XXXIII (TRANSDUCERS & EUROSENSORS XXXIII), Berlin, Germany, 2019, pp. 845-848
[30] Infineon, "Sillicon germanium 24GHz transceiver MMIC," BGT24MTR11 datasheet, Mar. 2014.
[31] ILICON radar, "24-GHz Highly Integrated IQ Transceiver," TRX_024_046 datasheet, Oct. 2021.
[32] ANALOG DEVICES, "4-Channel, 24GHz, Receiver Downconverter" ADF5904 datasheet, Oct. 2021.

Han-Sol Kim received the B.S. degree in electronic engineering from Hanyang University, Seoul, Korea, in 2020, and M.S. degree from the Korea Advanced Institute of Science and Technology (KAIST), Daejeon, Korea, in 2022. He is currently pursuing the Ph.D. degree with Korea Advanced Institute of Science and Technology (KAIST), Daejeon, Korea.

His research areas are radar signal processing for radar sensor, detecting target, anti-jamming algorithm, radar system design.

Jiyeol Meang received the B.S. degree in electrical engineering from Oklahoma State University, Stillwater, OK, USA, in 2020 and the M.S. degree in electrical engineering from Korea Advanced Institute of Science and Technology (KAIST), Daejeon, Republic of Korea, in 2023. Since 2023, he has been working with smartphone R&D group, Samsung Electronics Co., Ltd, Republic of Korea as an Engineer.

His research interests include microwave circuits, RF front-end circuits, and millimeter-wave antenna.

Ju-Hye Kim received the B.S. degree in electronic engineering from Ajou University, Suwon, Korea, in 2012 and MS degree in electronic engineering from Ajou University, Suwon, Korea, in 2014. She has been currently an assistant research engineer at Poongsan Defense R&D Institute since 2015. Her research interests include FMCW radar system and electronic system integration.

Dong-Sik Ko received the B.S. degree in electronic engineering from Dongguk University, Seoul, Korea, in 2007, and the M.S. degree in electronic engineering from Dongguk University, Seoul, Korea, in 2009, and the Ph.D degree in electronic engineering from Dongguk University, Seoul, Korea in 2013. He has been with the Millimeter-wave INnovation Technology Research Center (MINT), Seoul, Korea from 2007 to 2013, He has been currently a senior engineer at Poongsan Defense R&D Institute, Daejeon, Korea, since 2014.
His main focus is on the FMCW radar system, RF system, and electronic system integration.

Seong-Ho Seo received the B.S. degree in electronic engineering from the Kumoh National Institute of Technology, Kumi, Korea, in 1999, and M.S. degree in electronic radio information and communication engineering form the Chungnam National University, Daejeon, Korea, in 2009. He has been team leader Poongsan defense R&D institute, Deajeon, Korea, since 2000.
His research areas are high current circuit design and electromechanical system integration.

Muhammad Tayyab Azim was born in Pakistan in 1987. He received his B.E. degree in avionics engineering from the National University of Sciences and technology(NUST), Islamabad, Pakistan in 2009, M.S degree in Electrical Engineering from University of Surrey, Guildford, UK in 2011 and PhD. from KAIST Daejeon, South Korea in 2020. He is with the Microwave and Antenna Laboratory, School of Electrical Engineering, Korea Advanced Institute of Science and Technology (KAIST), Daejeon 34141, South Korea. His research interests include electromagnetics, antenna design, microwave components design, Electronic Warfare (EW), SAR and RADARS.

Seong-Ook Park received the B.S. degree in electrical engineering from Kyungpook National University, Daegu, Korea, in 1987, and the M.S. degree in electrical engineering from Korea Advanced Institute of Science and Technology (KAIST), Daejeon, in 1989, and the Ph.D. degree in electrical engineering from Arizona State University, Tempe, AZ, USA in 1997, under the supervision of Professors Constantine A. Balanis.

From March 1989 to August 1993, he was a Research Engineer with Korea Telecom, Daejeon, working with microwave systems and networks. He later joined the Telecommunication Research Center, Arizona State University, until September 1997. He is a member of Phi Kappa Phi Scholastic Honor Societies.

He has been a member of the faculty at the Information and Communications University from October 1997 to 2008, and has been currently a full professor since 2009 at KAIST. He has over 200 publications in refereed journals. He served as the Director General, Satellite Technology Research Center, KAIST from 2016 to 2018. He also served as President of The Korean Institute of Electromagnetic Engineering and Science (KIEES) in 2022. He has studied the improvement of antenna function inside of handset platforms, analytical and numerical techniques in the area of electromagnetics wave, and the precision technique of antenna measurement. His main focus is on the drone detection radar, SAR Payload, and the antenna system.